Bimeron nanoconfined design

I. A. Iakovlev, O. M. Sotnikov, and V. V. Mazurenko
Theoretical Physics and Applied Mathematics Department, Ural Federal University, Mira Street 19, Ekaterinburg 620002, Russia

(Received 24 January 2018; revised manuscript received 9 April 2018; published 11 May 2018)

We report on the stabilization of the topological bimeron structures in confined geometries. The Monte Carlo simulations for a ferromagnet with a strong Dzyaloshinskii-Moriya interaction revealed the formation of a mixed skyrmion-bimeron phase at finite temperatures. The vacancy grid created in the spin lattice drastically changes the picture of the observed spin configurations and allows one to choose between the formation of a pure bimeron and skyrmion lattice. We found that the rhombic plaquette provides a natural environment for stabilization of the bimeron structures. Such a rhombic geometry can protect the topological state even in the absence of the magnetic field.

DOI: 10.1103/PhysRevB.97.184415

I. INTRODUCTION

A specific shape of an object plays an important role in nature. One of the famous examples is the avian egg shape, whose significant variation in degree of asymmetry and ellipticity was recently related to flight adaptation of birds [1]. Another fascinating example is exoskeletons of viruses that are in the forms of the Platonic solids such as icosahedron [2], which provides the best and fastest connection of the subunits. There are also numerous examples when the particular shape choice revolutionized different fields of science or technology. In the first point-contact transistor invented by Bardeen and Brattain [3] a triangular form of the contact with one sliced tip was realized. It is important that the final shape of the system is formed via a trial and error process during evolution or engineering independently on the origin of the system.

Here we address the problem of the system shape choice on the level of the topologically protected magnetic structures [4,5] that attract considerable attention due to their potential technological applications in spintronics. The focus in this field of research gradually shifts from the study of the bulk crystals characterized by infinite skyrmion lattices [6,7] to confined geometries [8,9] with isolated topological spin configurations that can be controlled by means of electric and magnetic fields [10]. A practical realization of the skyrmion-based device with a strongly confined nanodisk geometry was recently reported in Ref. [8]. The authors of the work have demonstrated switching between different stable skyrmionic states in a 160-nm-diameter FeGe nanodisk. These experimental results stimulated the theoretical search for other confined geometries [11].

The scanning tunneling microscopy (STM) allows one to manipulate individual atoms deposited on the surface and provides access to a completely different scale of the confined magnetic geometries with size of several nanometers. In this sense clusters or plaquettes of magnetic atoms constructed by means of the STM [12] on a surface can be considered as an elementary unit cell for stabilization of the topologically protected excitations. Moreover, the local spin current from a scanning tunneling microscope can be used to write and to delete individual skyrmions, as was shown in Ref. [13].

In this paper we demonstrate that the choice of the rhombic shape of the spin plaquette is important to stabilize a distinct type of topological structures, bimerons [14] that consist of two merons (half-disk domain carrying the skyrmion number $Q = 1/2$) separated by a stripe domain with zero topological charge. According to Fig. 1 the pair of bimerons can be stabilized on rhombic clusters in a wide range of ratios between Dzyaloshinskii-Moriya interaction (DMI) and Heisenberg ferromagnetic exchange. Remarkably, being formed at the finite magnetic field, these topological spin structures remain stable with magnetic field switched off at very low temperatures, which is in demand for creating new atomic-memory technologies. At the same time, in the case of the two-dimensional square lattice the magnetic bimerons can be segregated in a fully controllable way with a vacancy grid.

II. MODEL AND METHOD

Hamiltonian. In our study we used the following spin Hamiltonian for simulations of the topological magnetic spin configurations on the $L \times L$ square lattices:

$$H = -\sum_{i<j} J_{ij}\mathbf{S}_i \cdot \mathbf{S}_j - \sum_{i<j} \mathbf{D}_{ij} \cdot [\mathbf{S}_i \times \mathbf{S}_j] - \sum_i B S_i^z, \quad (1)$$

where J_{ij} and $\mathbf{D}_{ij}$ are the isotropic interaction and Dzyaloshinskii-Moriya vector, respectively. $\mathbf{S}_i$ is a unit vector along the direction of the ith spin and B denotes the out-of-plane magnetic field. We take into account the interaction only between nearest neighbors. The summation for interspin couplings runs once over every pair. The isotropic exchange interaction is positive in our simulations, which corresponds to the ferromagnetic case. The symmetry of the Dzyaloshinskii-Moriya vectors is of C_{4v} type; DMI has an in-plane orientation and is perpendicular to the corresponding intersite radius vector, $\mathbf{r}_{ij} = \mathbf{r}_j - \mathbf{r}_i$.

Since the values of the Dzyaloshinskii-Moriya interaction used in our simulations are equal or larger than the isotropic exchange interaction, then the resulting skyrmion species are compact. The possible realization of such an interaction regime was recently demonstrated in Ref. [15] by means of

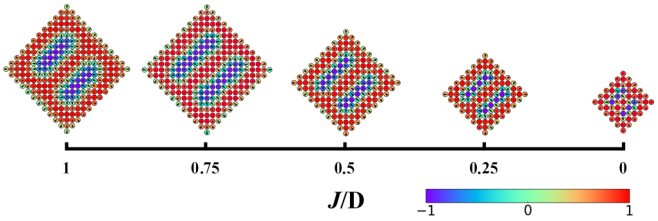

FIG. 1. Family of the rhombic plaquettes with bimeron pairs stabilized in Monte Carlo simulations of systems described by the spin Hamiltonian, Eq. (1). Calculations were performed at different ratios $\frac{J}{|\mathbf{D}|}$ ranging from 0 to 1. Magnetic atoms are represented by circles, black arrows denote the xy-plane projections of the spin moments, and color shows the z component of the spin. The magnetic field in these simulations was chosen to be 0.22, 0.3, 0.4, 0.7, and 1.3 for the plaquettes from left to right, respectively. The temperature is equal to 0.014. All the parameters are in units of DMI.

high-frequency laser fields. On the other hand, there are surface nanosystems [16] with sp electrons that are naturally characterized by a strong suppression of the isotropic interaction.

Monte Carlo approach. To solve the spin Hamiltonian, Eq. (1), we use the Monte Carlo approach with GPU parallelization [17–19]. It gives us an opportunity to achieve significant acceleration of the Monte Carlo simulations up to 5–200 times compared to the CPU analogs [17,18]. For example, we can perform simulations of large-scale two-dimensional systems with linear sizes up to $L = 1024$. Since each spin in our model interacts only with nearest neighbors, we chose the spin update scheme within the Metropolis algorithm of checkerboard type. During Monte Carlo (MC) simulations, we gradually cooled down the system from $T = 1.0J$. The number of temperature steps was equal to 50. Each run comprises 1.5×10^5 MC steps per spin. Simulation parameters in a similar range were used in Ref. [20].

Topological charge. To calculate the skyrmion number (topological charge) denoted as Q we adopted the approach proposed in Refs. [21,22],

$$Q = \frac{1}{4\pi}\sum_l A_l, \tag{2}$$

where A_l is the solid angle subtended by three spins located at the vertices of an elementary triangle l,

$$A_l = 2\arccos\left(\frac{1+\mathbf{S}_i\cdot\mathbf{S}_j+\mathbf{S}_j\cdot\mathbf{S}_k+\mathbf{S}_k\cdot\mathbf{S}_i}{\sqrt{2(1+\mathbf{S}_i\cdot\mathbf{S}_j)(1+\mathbf{S}_j\cdot\mathbf{S}_k)(1+\mathbf{S}_k\cdot\mathbf{S}_i)}}\right). \tag{3}$$

The sign of A_l in Eq. (2) is determined as $\mathrm{sgn}(A_l) = \mathrm{sgn}(\mathbf{S}_i \cdot [\mathbf{S}_j \times \mathbf{S}_k])$. Importantly, we do not consider the exceptional configurations for which

$$\mathbf{S}_i \cdot [\mathbf{S}_j \times \mathbf{S}_k] = 0; 1 + \mathbf{S}_i\cdot\mathbf{S}_j + \mathbf{S}_j\cdot\mathbf{S}_k + \mathbf{S}_k\cdot\mathbf{S}_i \leqslant 0. \tag{4}$$

Spin structure factor. Other important observables that can be used for identification of magnetic phases are the spin structure factors given by

$$\chi_\parallel(\mathbf{q}) = \frac{1}{N}\left\langle\left|\sum_i S_i^z e^{-i\mathbf{q}\mathbf{r}_i}\right|\right\rangle, \tag{5}$$

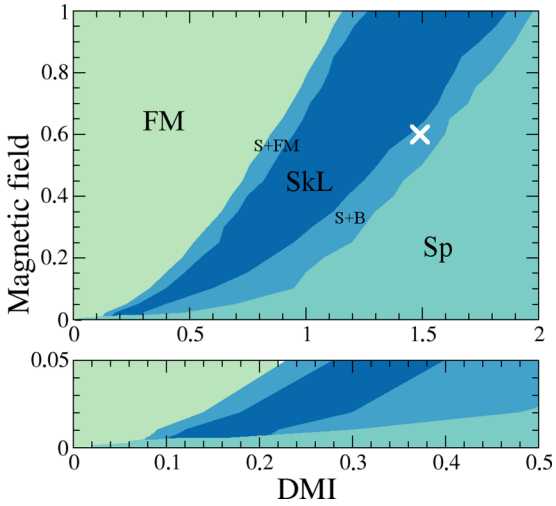

FIG. 2. Top panel: Phase diagram of the ferromagnet with Dzyaloshinskii-Moriya interaction. The abbreviations SkL, S+FM, S+B, FM, and Sp denote skyrmion lattice state, nonperiodic skyrmion state, mixed phase of skyrmions with bimerons, ferromagnetic, and spin spiral states, respectively. The phase diagram was obtained by using the simulations for lattices of 256×256 at $T = 0.02$. Bottom panel: Fragment of the full phase diagram corresponding to the weak magnetic fields $B < 0.05$ and Dzyaloshinskii-Moriya interactions $|\mathbf{D}| < 0.5$. All the parameters are given in units of isotropic exchange interaction.

$$\chi_\perp(\mathbf{q}) = \frac{1}{N}\left\langle\left|\sum_i S_i^x e^{-i\mathbf{q}\mathbf{r}_i} + \sum_i S_i^y e^{-i\mathbf{q}\mathbf{r}_i}\right|\right\rangle, \tag{6}$$

where $\mathbf{q}$ is the reciprocal space vector, S_i^α $[\alpha = (x,y,z)]$ is the projection of the ith spin, and $\mathbf{r}_i$ is the radius vector for the ith site.

Phase diagram. To construct the phase diagram we used a 100×200 grid (20 000 points in total) on the magnetic field/DMI plane. For each point we carried out 15 Monte Carlo runs. Thus, the total number of Monte Carlo calculations was equal to 300 000. To identify the different phases realized in the system we used the calculated topological charge, Eq. (2), spin structure factors, Eqs. (5) and (6), and visualized a number of magnetic configurations during Monte Carlo simulations.

To test the stability of the phase classification results we have varied the number of Monte Carlo steps in our simulations from 10^4 to 50×10^4 per spin. To check the sensitivity of the obtained results to the cooling procedure we varied the maximal temperature from $0.5J$ to $5J$ and the number of the temperature steps from 20 to 150. All these additional simulations confirm the stability and correctness of the phase diagram results presented in Fig. 2.

III. RESULTS

Regular lattice. The first step of our investigation is to construct a phase diagram (Fig. 2) for the spin Hamiltonian, Eq. (1). The corresponding numerical details are presented in the previous section. Figure 3 gives the typical examples of the spin structure factors corresponding to the different phases. One can see that the different magnetic phases can be uniquely

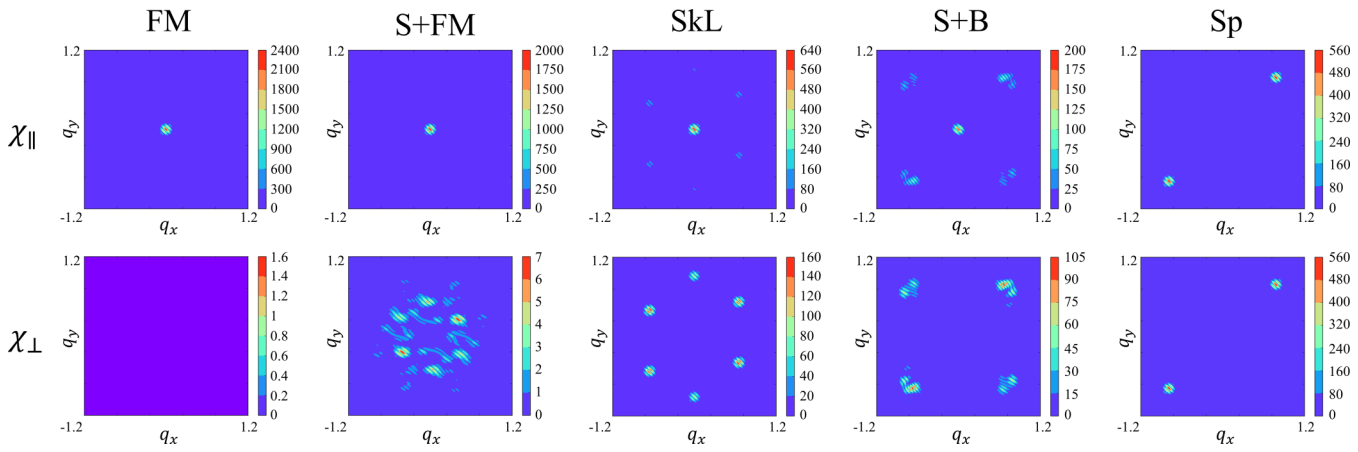

FIG. 3. Structure factors of different phases observed in the system under consideration. These results were obtained at $B = 0.5J$ and $|\mathbf{D}| = 0.7J$ (FM), $0.77J$ (S+FM), J (SkL), $1.4J$ (S+B), $1.5J$ (Sp).

identified from the inspection of the pictures of intensities. For instance, the in-plane structure factor of mixed skyrmion-bimeron and skyrmion phases is characterized by double-**q** and triple-**q** states, respectively. In turn, all the skyrmionic phases are characterized by a nonzero topological charge value.

According to the results presented in Fig. 2 (bottom panel), at zero magnetic field we observe the formation of the spin spiral state for $|\mathbf{D}|/J > 0.01$, which is in agreement with analytical solution, and previous numerical and experimental results [23].

The phase diagram plot [Fig. 2 (top panel)] shows that the skyrmion phase is composed of a nonperiodic skyrmion (S+FM) state, a periodic skyrmion lattice (SkL), and a mixed state of skyrmions and bimerons (S+B). Our main focus is on the S+B phase, since we search for the conditions of pure bimeron structure stabilization. A typical example of the magnetic configuration corresponding to the S+B phase is presented in Fig. 4 (top panel). The bimerons of different sizes are located along the diagonals of the square lattice with periodic boundary conditions. From the calculated topological charge density plot, Fig. 4 (bottom panel), one can see that each bimeron contains two merons and a rectangular stripe domain in the middle part.

A similar mixed phase was simulated in Ref. [14] with the two-dimensional nonlinear sigma model and was experimentally observed at low temperatures in itinerant ferromagnets with Dzyaloshinskii-Moriya interaction [23]; however, it was identified as a combination of skyrmions and fragments of helices. At the same time, from analytical calculations [24,25] it is known that the mixed regimes do not represent the ground state of the system at zero temperature, where only the spin spiral, skyrmion lattice, and ferromagnetic phases can be observed. Such a difference between analytical and numerical solutions is due to the temperature effects. Indeed, as was shown in Ref. [14] the meron phase appears at finite temperature, since its entropy is much larger than that of the spin spiral or skyrmion phase.

The width of observed bimerons corresponds to the diameter of the skyrmion. The latter is controlled by the $\frac{J}{|\mathbf{D}|}$ ratio. The mean length of bimerons increases with an increase of DMI strength at a fixed magnetic field. On the other hand, the bimeron length decreases with an increase of the magnetic field value at the fixed DMI. In such a system setup it is impossible to predict an exact length and location of a bimeron, which is our main interest in this study.

Vacancy grid. The effect of point defects on the skyrmionic lattice state attracts considerable attention mainly due to the possibility to observe magnetic monopoles [26] predicted by Dirac. Experimentally, it was also shown [27] that inlayer and

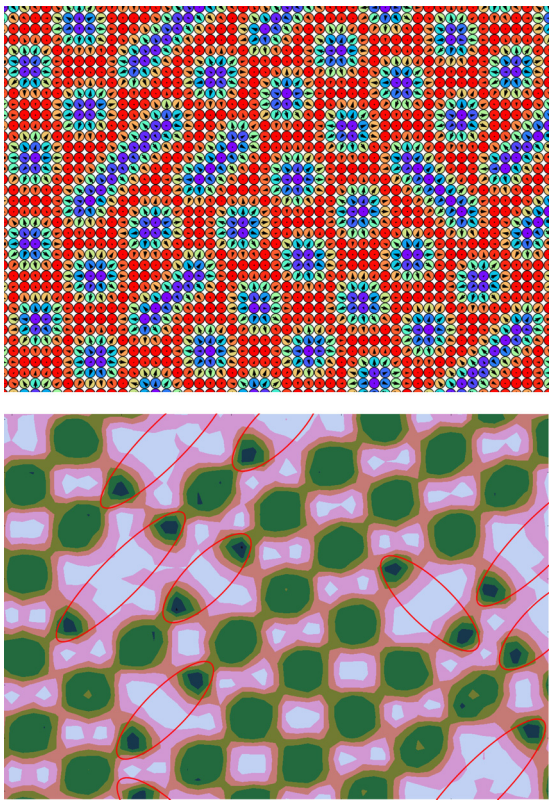

FIG. 4. Top panel: Fragment of the square lattice with $L = 512$ demonstrating the Monte Carlo solution obtained with the parameters $B = 0.6$, $|\mathbf{D}| = 1.5$, $T = 0.02$ (white cross in Fig. 2), which corresponds to the S+B phase. Bottom panel: The calculated topological charge density. Bimerons are marked with red ovals. All the parameters are given in units of isotropic exchange interaction.

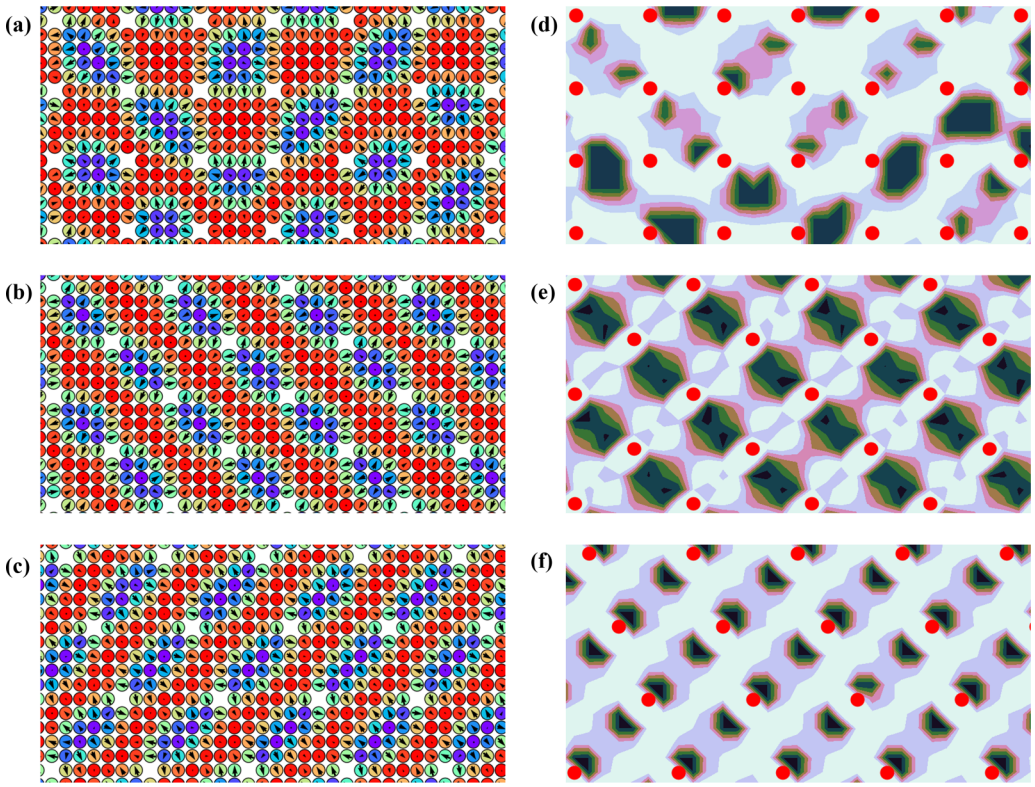

FIG. 5. Fragments of the square lattice with $L = 512$ demonstrating the Monte Carlo solution of the spin model, Eq. (1), in the presence of a periodic vacancy grid with cells in the form of squares (a), rhombus (b), and parallelogram (c). (d)–(f) give the corresponding topological charge densities. Simulations were carried out at $B = 0.4$, $J = 0.67$, $T = 0.014$ [white cross in Fig. 2 (top panel)]. All the parameters are given in units of DMI.

adatom defects in surface nanostructures can modify the energy landscape and can be used for moving individual skyrmions in the STM experiments.

Previous numerical studies [20] on the discrete lattices revealed the formation of the bimerons in the presence of the vacancies randomly distributed over the system. As proposed in Ref. [20] on the basis of the previous theoretical [14] and experimental [26] works, the presence of spin vacancies is equivalent to the local magnetic field term in the spin Hamiltonian. In this sense, the authors of Ref. [20] identified the mechanism of the bimeron stabilization as the impact of effective local magnetic fields introduced by spin vacancies. However, a probabilistic formation of bimerons prevents one from using such a system in practical applications. In this work we mainly focus on the study of the topological spin configurations in systems where vacancies have regular positions, which opens a way for the creation of atomic-scale memory units. In this respect, recent STM experiments [28] demonstrated an

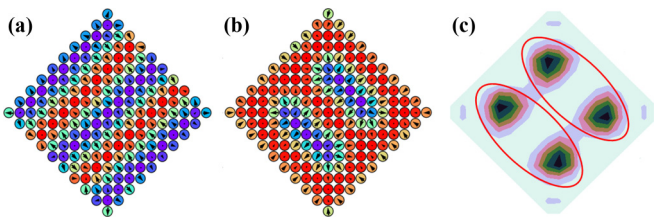

FIG. 6. Monte Carlo solutions of the spin model, Eq. (1), on the rhombic plaquette at $B = 0$ (a) and $B = 0.4$ (b). (c) The topological charge density corresponds to (b). Bimerons are marked with red ovals. Here $J = 0.67$, $T = 0.014$. All the parameters are given in units of DMI.

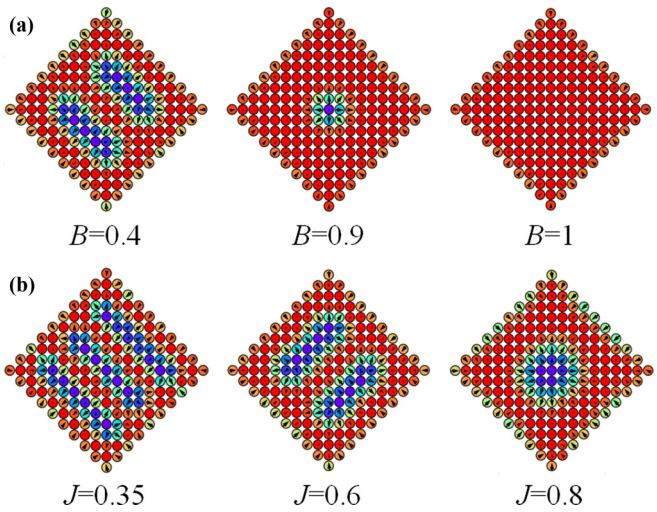

FIG. 7. (a) Dependence of the Monte Carlo solution on the magnitude of the magnetic field. Here $J = 0.67$, $T = 0.014$. (b) Dependence of the topological structures on the $\frac{J}{|\mathbf{D}|}$ ratio. Here $B = 0.45$, $T = 0.014$. All the parameters are given in units of DMI.

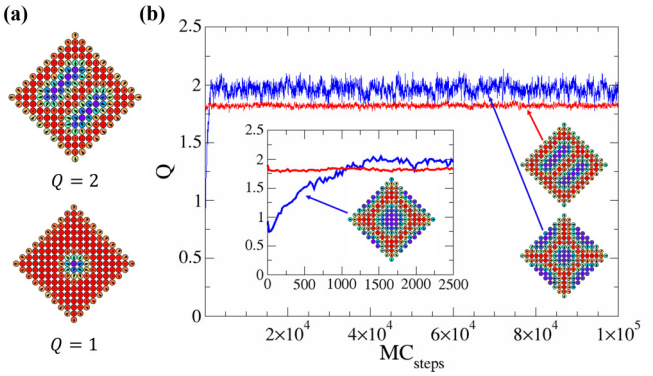

FIG. 8. Demonstration of solution stability. (a) The bimeron (top) and skyrmion (bottom) magnetic configurations obtained at $B = 0.4$ and $B = 0.9$, respectively. Here, $T = 0.005$ and $J = 0.67$. (b) Time evolution of the prepared bimeron and skyrmion states after switching the field off. The inset shows short-time evolution of the topological structures. All the parameters are given in units of DMI.

unprecedented possibility to manipulate the vacancies in the surface nanosystems for high-density storage of information.

Here we used a similar idea for stabilization of the bimerons on the two-dimensional lattice. To demonstrate the effect of vacancies insertion we choose the Hamiltonian parameters near the border between the SkL and S+B phases. The corresponding Monte Carlo solution for the lattice without vacancies presented in Fig. 4 shows that the system is mainly filled by the skyrmions with several bimeron structures. For the same set of parameters the regular square grid of vacancies created in the spin lattice leads to the formation of the bimerons of the same size. However, there is still a fraction of the skyrmions [Figs. 5(a) and Fig. 5(d)]. We found that the size of the square vacancy grid cell should be close to the period of the spin spiral in the initial lattice without defects. For instance, in the considered case the diagonal of the vacancies grid cell is equal to $5\sqrt{2}$ in the units of the lattice constant, while the period of the spin spiral is $4\sqrt{2}$. With a further increase in length, the bimerons also arise, but these configurations do not exhibit a stable appearance of such spin structures.

A pure skyrmion or pure bimeron lattice can be stabilized by forming a vacancy grid with rhombic or parallelogram unit cells. As is demonstrated in Figs. 5(b) and Fig. 5(c) the choice between pure bimeron and skyrmion phases can be made by choosing the corresponding shape of the vacancy grid cell. Importantly, the size of the grid cell must also be adjusted to the spin spiral period length. For instance, the number of magnetic atoms on the shorter diagonal of the parallelogram is four, which is close to the period of spin spiral ($4\sqrt{2}$) formed on the nondefective initial lattice at zero magnetic field.

Rhombic plaquette. Having simulated the lattices with periodic boundary conditions, we are in a position to find a shape of a finite spin cluster in which the pure bimeron states are stabilized at finite temperatures and magnetic fields. Figure 6 demonstrates such a plaquette that is a rhombic fragment of the square lattice. At zero magnetic field we observe a spin spiral state, Fig. 6(a). At constant ratio $J/|\mathbf{D}|$, the plaquette state can be switched between a bimeron pair, a single skyrmion, and a fully polarized case by variation of the external magnetic field [Fig. 7(a)].

In turn, the different values of the isotropic exchange interaction at the fixed magnetic field of $0.45|\mathbf{D}|$ can produce three-bimeron, two-bimeron, or skyrmion state, as can be seen from Fig. 7(b).

One of the fascinating properties of the spin clusters with rhombic shape is that bimeron spin structures remain stable when the magnetic field is instantly switched off. According to the Monte Carlo results presented in Fig. 8, the skyrmion number of the plaquette with starting bimeron configuration fluctuates around 1.8, which is slightly smaller than the saturated value of 2 at the finite magnetic field. In turn, the single skyrmion stabilized at the magnetic field of $0.9|\mathbf{D}|$ transforms into another structure with nonzero topological charge when the magnetic field is switched off. As can be seen from Fig. 8(b), the new structure is characterized by one skyrmion in the center of the plaquette and boundary spins that are parallel to the skyrmion core magnetization. According to our simulation results, strong fluctuations of the topological charge are mainly related to fluctuations of the orientation of the boundary spins.

Since without magnetic field such a bimeron state corresponds to the local minimum of the system, it can be destroyed by temperature fluctuations. For instance, the systems visualized in Fig. 8(a) relax to a spin spiral state when the temperature is increased from 0.005 to $0.012|\mathbf{D}|$ (for the bimeron pair state) or to $0.025|\mathbf{D}|$ (for the skyrmion state). These results are sensitive to the details of the Monte Carlo simulations. For instance, in our scheme the new direction of a spin is chosen by using the solid angle restriction of 10°.

At last, the stability of the bimerons structures in the connected rhombic clusters should be investigated in order to use such systems in real applications, for instance as a building block of nanoscale memory devices. The results for the two-plaquette configurations with different number of boundary spins having nearest neighbors belonging to another plaquette are visualized in Fig. 9. The stable bimeron

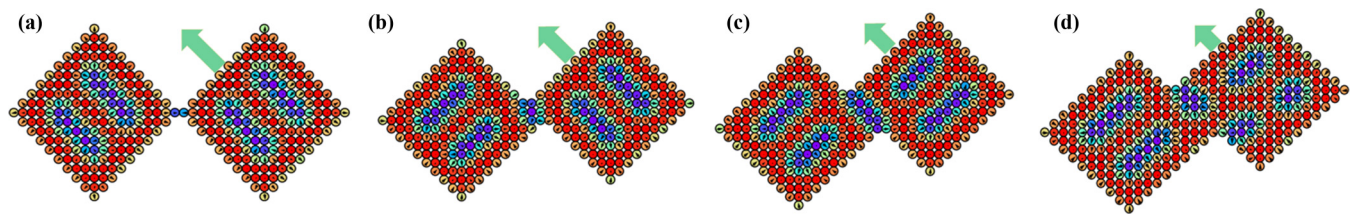

FIG. 9. Example of connections between two rhombic plaquettes carrying a pair of bimerons. The number of contacting spins is one, three, five, and six for (a)–(d), respectively. The parameters used in these simulations are $J = 0.67$, $T = 0.014$. The arrow denotes the direction of the shift of the plaquettes with respect to each other. All the parameters are given in units of DMI.

configurations in both plaquettes having 19 diagonal spins exist while the number of contacting spins is less than six. We have checked that the complete linking of two plaquettes leads to the formation of a mixed skyrmion-bimeron state.

IV. CONCLUSIONS

We have shown that the two-dimensional bimeron lattice can be stabilized in a controllable way by means of the regular vacancies grid created in the spin lattice with competing Dzyaloshinskii-Moriya and isotropic exchange interactions. The size and shape of the vacancy grid cell define the type and length of the topological magnetic structures in the spin system. In the limiting case of the finite spin cluster one needs to choose the rhombic shape to guarantee the formation of bimerons. The obtained results can be used to guide future scanning tunneling microscopy experiments aiming to control the topological spin configurations in confined nanostructures.

ACKNOWLEDGMENTS

We thank Alexander Tsirlin for fruitful discussions. This work was supported by the Russian Science Foundation, Grant No. 17-72-20041.

[1] M. C. Stoddard, E. H. Yong, D. Akkaynak, C. Sheard, J. A. Tobias, and L. Mahadevan, Science **356**, 1249 (2017).
[2] F. Wilczek, *A Beautiful Question: Finding Nature's Deep Design* (Penguin Press, New York, 2015).
[3] J. Bardeen, *Semiconductor Research Leading to the Point Contact Transistor*, Nobel lecture (Elsevier, Amsterdam, 1956); W. H. Brattain, *Surface Properties of Semiconductors*, Nobel lecture (Elsevier, Amsterdam, 1956).
[4] S. Mühlbauer, B. Binz, F. Jonietz, C. Pfleiderer, A. Rosch, A. Neubauer, R. Georgii, and P. Böni, Science **323**, 915 (2009).
[5] A. N. Bogdanov and D. A. Yablonsky, Sov. Phys. JETP **95**, 178 (1989).
[6] F. Jonietz, S. Mühlbauer, C. Pfleiderer, A. Neubauer, W. Münzer, A. Bauer, T. Adams, R. Georgii, P. Böni, R. A. Duine, K. Everschor, M. Garst, and A. Rosch, Science **330**, 1648 (2010).
[7] A. Neubauer, C. Pfleiderer, B. Binz, A. Rosch, R. Ritz, P. G. Niklowitz, and P. Böni, Phys. Rev. Lett. **102**, 186602 (2009).
[8] F. Zheng, H. Li, S. Wang, D. Song, C. Jin, W. Wei, A. Kovács, J. Zang, M. Tian, Y. Zhang, H. Du, and R. E. Dunin-Borkowski, Phys. Rev. Lett. **119**, 197205 (2017).
[9] H. Du, W. Ning, M. Tian, and Y. Zhang, Europhys. Lett. **101**, 37001 (2013).
[10] W. Koshibae, Y. Kaneko, J. Iwasaki, M. Kawasaki, Y. Tokura, and N. Nagaosa, Jpn. J. Appl. Phys. **54**, 053001 (2015).
[11] R. A. Pepper, M. Beg, D. Cortés-Ortuno, T. Kluyver, M.-A. Bisotti, R. Carey, M. Vousden, M. Albert, W. Wang, O. Hovorka, and H. Fangohr, J. Appl. Phys. **123**, 093903 (2018).
[12] S. Loth, Susanne Baumann, Christopher P. Lutz, D. M. Eigler, and Andreas J. Heinrich, Science **335**, 196 (2012).
[13] N. Romming, C. Hanneken, M. Menzel, J. E. Bickel, B. Wolter, K. von Bergmann, A. Kubetzka, and R. Wiesendanger, Science **341**, 636 (2013).
[14] M. Ezawa, Phys. Rev. B **83**, 100408(R) (2011).
[15] E. A. Stepanov, C. Dutreix, and M. I. Katsnelson, Phys. Rev. Lett. **118**, 157201 (2017).
[16] V. V. Mazurenko, A. N. Rudenko, S. A. Nikolaev, D. S. Medvedeva, A. I. Lichtenstein, and M. I. Katsnelson, Phys. Rev. B **94**, 214411 (2016).
[17] M. Weigel and T. Yavorskii, Phys. Procedia **15**, 92 (2011).
[18] M. Weigel, Phys. Commun. **182**, 1833 (2011).
[19] M. Bernaschi, G. Parisi, and L. Parisi, arXiv:1006.2566.
[20] R. L. Silva, L. D. Secchin, W. A. Moura-Melo, A. R. Pereira, and R. L. Stamps, Phys. Rev. B **89**, 054434 (2014).
[21] B. Berg and M. Lüscher, Nucl. Phys. B **190**, 412 (1981).
[22] C. Heo, N. S. Kiselev, A. K. Nandy, S. Blügel, and T. Raising, Sci. Rep. **6**, 27146 (2016).
[23] X. Z. Yu, Y. Onose, N. Kanazawa, J. H. Park, J. H. Han, Y. Matsui, N. Nagaosa, and Y. Tokura, Nature (London) **465**, 901 (2010).
[24] A. Bogdanov and A. Hubert, J. Magn. Magn. Mater. **138**, 255 (1994).
[25] A. Bogdanov and A. Hubert, Phys. Status Solidi B **186**, 527 (1994).
[26] P. Milde, D. Köhler, J. Seidel, L. M. Eng, A. Bauer, A. Chacon, J. Kindervater, S. Mühlbauer, C. Pfleiderer, S. Buhrandt, C. Schütte, and A. Rosch, Science **340**, 1076 (2013).
[27] C. Hanneken, A. Kubetzka, K. von Bergmann, and R. Wiesendanger, New J. Phys. **18**, 055009 (2016).
[28] F. E. Kalff, M. P. Rebergen, E. Fahrenfort, J. Girovsky, R. Toskovic, J. L. Lado, J. Fernández-Rossier, and A. F. Otte, Nat. Nanotechnol. **11**, 926 (2016).